Desalination 467 (2019) 229–244

Contents lists available at ScienceDirect

Desalination

journal homepage: www.elsevier.com/locate/desal

Proposal and assessment of a novel hybrid system for water desalination using solar and geothermal energy sources

V. Okati[a,b,c,*], Amir Ebrahimi-Moghadam[b,**], A. Behzadmehr[a], Mahmood Farzaneh-Gord[d]

[a] Mechanical Engineering Department, University of Sistan and Baluchestan, Zahedan 981-35161, Iran
[b] Faculty of Mechanical Engineering, Shahrood University of Technology, Shahrood, Iran
[c] Faculty of Marine Engineering, Chabahar Maritime University, Chabahar 9971756499, Iran
[d] Faculty of Engineering, Mechanical Engineering Department, Ferdowsi University of Mashhad, Mashhad, Iran

GRAPHICAL ABSTRACT

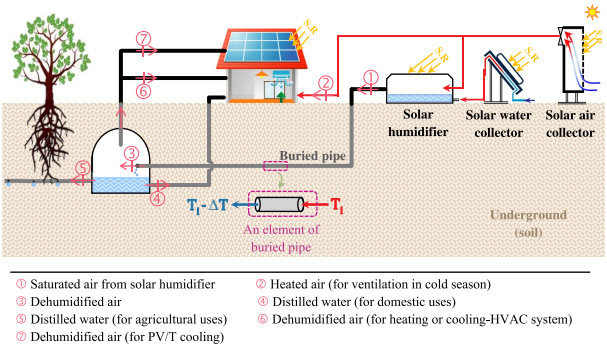

ARTICLE INFO

Keywords:
Solar desalination
Solar humidification-dehumidification cycle
Geothermal energy
Ground heat exchanger
Solar collector

ABSTRACT

The Earth's radiation potential and solar energy can be suitable alternatives to other nonrenewable energies. This work presents the study of solar desalination unit compounded with ground heat exchanger. The amount of freshwater produced by the unit is assessed by solving mass and energy balance equations for the cycle's various sections including air and water solar collectors, solar humidifier and ground heat exchanger. Findings indicate that under given conditions, using a solar collector increases freshwater production by 30.35%, whereas using air solar collector increases it by 4.45% only. In addition, since the temperature of outlet air from the ground heat exchanger has a constant value during various seasons of the year at a depth of 1 m under the ground, this air flow can be harnessed to increase productivity in solar photovoltaic and heating, ventilation, and air conditioning (HVAC) cycles. The results of this paper could be considered as a step forward for producing freshwater even during nighttime (when there is no solar radiation) in regions with humid climate.

1. Introduction

Water and energy have always played pivotal roles in urban development; social health and economic development of countries depend on energy and procuring safe and healthy water. On the other side, increasing environmental pollution increases the need of using

* Corresponding author at: Mechanical Engineering Department, University of Sistan and Baluchestan, Zahedan 981-35161, Iran.
** Correspondence to: A. Ebrahimi-Moghadam, Faculty of Mechanical Engineering, Shahrood University of Technology, Shahrood, Iran.
E-mail addresses: vahab_okati@yahoo.com (V. Okati), amir_ebrahimi_051@shahroodut.ac.ir, amir_ebrahimi_051@yahoo.com (A. Ebrahimi-Moghadam).

https://doi.org/10.1016/j.desal.2019.06.011
Received 13 February 2019; Received in revised form 15 May 2019; Accepted 17 June 2019

renewable energies such as solar energy for producing freshwater. Although there is freshwater in most of the world, it is not available in the form of drinking water and there is a shortage thereof. There is an increasing demand for water, while existing freshwater resources are not enough to meet human needs. Pollution of rivers and lakes due to disposal of urban and industrial waste has aggravated freshwater shortage. Global development and rapid growth of world population have dramatically increased the need for freshwater resources to the extent that the world will have to deal with water shortage by 2020 [1,2]. Access to freshwater has become a national and international issue all around the world. Desalination industries can offer us alternative sources of available water such as seawater or brackish water. By 2020 the issue of water will be a major crisis for many countries [3].

Desalination processes require much energy; the energy required by these processes is supplied directly or indirectly from fossil fuels. These fuels not only levy considerable costs on desalination process, but also directly or indirectly inflict adverse environmental damages. It is both economically and environmentally reasonable and desirable to find ways to use renewable energies for desalination process, especially solar and geothermal energies. To procure freshwater in areas that are facing freshwater shortage and only have common energy resources (e.g. electricity and heat) available to them, adopting desalination technologies which utilize renewable energies could be a viable option. In recent years, using renewable energies for water desalination has been increasingly recognized as a viable option and desalinators using these energies are operative throughout the world. Most of these desalinators are designed and launched for arid areas and generally utilize solar energy, wind or geothermal energy for freshwater production.

One of the most significant recent breakthroughs in solar desalination systems is using humidification-dehumidification of air [4], originally developed by Bourouni et al. [5]. This technique is based on the fact that air can mix with huge amount of vapor and air's ability to carry vapor increases with temperature. When flowing air comes into contact with saline water, certain amount of vapor is absorbed by air which needs to be cooled in order to be condensed; this vapor condensation occurs in the condenser (GHE-ground heat exchanger).

As mentioned before, the system which is the subject of the present study consists of a humidification section with its other related functions and a dehumidification section for freshwater production. Unlike other renewable energies, the ground's latent heat is not limited to particular season, time or conditions and may be constantly exploited. Shallow geothermal energy, as an available clean renewable energy source, has been increasingly considered and applied [6]. Ground heat exchanger which takes shallow geothermal energy as heat source/heat sink is widely used and has proven to be highly efficient [7,8].

In climates where ground temperature range is close to human comfort temperature (15–23 °C), this low temperature can be harnessed in shallow depths of the ground for cooling or transferring the heat from different parts of the system's equipment to the ground. However, the cooling effect is negligible in areas where ground heat is higher than the ambient temperature. Using ground heat exchangers can nevertheless be a good alternative to fossil fuels for producing hot water or heat to be used in power plants, houses or farming; it causes decreasing the amount of greenhouse gases in environment. Many studies have been done about decreasing the amount of greenhouse gases [9–11].

The Earth's heat exchange capacity is very high. Studies show that when the earth is used as heat collector and dissipater, the temperature of the soil surrounding heat exchangers increases only marginally. The study by Shuhong Li shows that the temperature of the soil surrounding a subsurface heat exchanger used in an air conditioning system increased 2.56–3.00°C after 15 years [6]. Lindblom et al. have reported similar results in their experiments [12]. Their research shows that the amount of freshwater produced in the early days of the experiment decreases drastically, but reaches a steady production rate after a 90-day period, which indicates that the temperature of the soil surrounding the tubes remains constant. One of the applications of ground heat exchangers is in passive and active ventilation systems. Since there is steady temperature in a depth of 2–4 m beneath the earth, we may employ the Earth's heat capacity for cooling or heating in summer or winter by flowing fresh atmosphere air through buried tubes and heat transfer [7,13–18]. Combining a conventional air conditioner and an earth air heat exchanger (EAHE) can result in an 18.1% reduction in energy consumption [19]. Ground heat exchanger may also be utilized as a ground source heat pump (GSHP). In such a system, the ground heat exchanger has an important role in transferring heat between the fluid flowing through the tubes and the surrounding environment. GSHP systems are divided in two open and closed systems [20]. In open systems, GHE acquires cooling or heating energy directly through contact with underground or surface waters [21]. However, in a closed system which is usually referred to as ground coupled heat pump system (GCHP), the ground is directly used as heat source while the fluid flows through GHE [22].

GCHP system is itself divided into horizontal and vertical types [23]. In the vertical type, tubes are buried in a depth of 80 to 500 m, whereas in a horizontal system tubes are horizontally buried in a depth of 1.5 to 3 m. Due to its simple installation, the horizontal type is more inexpensive compared to the vertical type which requires more equipment for installation and implementation [24–26]. The heat exchanger under study is designed so that it can be used both as an earth air heat exchanger (EAHE) and as condenser in solar desalination cycle.

After conducting preliminary studies on the heat exchanger employed in this research project, humidification cycle and its components will now be reviewed.

The humidification-dehumidification (HDH) desalination process is, in fact, adopted from water's natural cycle in nature and is based on the fact that the air can mix with certain amount of water vapor. In addition, the amount of vapor present in the air can be increased by increasing its temperature. Solar still is a desalination system based on humidification-dehumidification cycle. Numerous studies have corroborated that using solar collectors coupled with solar stills increases the amount of water produced in solar stills [27–29]. In one of these studies, Badran et al. showed that using flat-plate solar collector can increase water production in solar still by 36% [30]. In another study, Okati et al. proved that increasing solar still's inlet water and air temperature results in boosted freshwater production [31,32]. Currently, however, humidification-dehumidification systems include a broad range of water desalination systems. Studies indicate that employing solar collectors in desalination systems results in increased production of freshwater [33–35]. In the study by Elatter et al., increasing the temperature and humidity of the system's inlet air increased their system's freshwater production [36,37].

In solar stills, freshwater is produced in the chamber itself through the condensation of water vapor on glass walls. However, new systems have been introduced in which vapor is condensed outside the solar still by external or internal condensers; this can increase solar still's freshwater output [38].

This work introduces a compound system for freshwater or irrigation water production and including a solar desalinator (solar still) as humidifier and a ground heat exchanger as condenser consisting of underground tubes in which humid air flows inside it. Analysis focuses on humid air condensation and the production of water in an unperforated tube (as main tube). The condensed water can be collected at the end of this main tube. The collected water can be used for drinking and also it can be guided through a perforated tube to the plant roots (agricultural uses). In addition, since the heat exchanger's outlet air reaches the temperature of the ground at the depth in which the condenser is buried, it may be used for cooling or heating houses depending on the season in which the system is operating. The purpose of this study is to investigate the impact of various design parameters on solar desalinator and ground condenser's productivity as well as the effect of using ground heat exchanger for cooling or heating purposes. Therefore, a suitable thermodynamic model is proposed to investigate

the cycle's operational conditions and equations related to solar desalinator and dehumidification unit are solved.

The use of a hybrid freshwater system consisting of just renewable energy sources causes an increase the system efficiency (increasing the amount of produced fresh water) and also reduction of the pollutants emissions; but very limited researches have been performed around it to the best of the authors' knowledge. Accordingly, in order to achieve these goals, conventional desalination system is combined with solar and geothermal energy equipment. The main components of the proposed system in current study are air/water solar collectors, solar humidifier and GHE. In summary, the innovations and highlights of this study are as follows:

- Since the temperature of the outlet air from the ground heat exchanger has a constant value during various seasons of the year at a depth of 1 m under the ground, this air flow can be harnessed to increase productivity in solar photovoltaic with cooling PV in warm seasons and this used for heating, ventilation, and air conditioning (HVAC) cycles.
- Considering the increase in the cycle's inlet air temperature by the air solar collector as well as by forced convection of air over the warm water in the solar humidifier and increasing of convection coefficient, vapor production in this system will be more than conventional solar stills.
- Simultaneous using of air and water solar collectors to increase freshwater production, and using these collectors for other purposes such as providing hot water for houses using secondary heat exchanger (water solar collector) and/or ventilation in cold seasons to increase house temperature (air solar collector) will be advantageous to the environment due to decreased energy consumption in the building and reduced CO_2 emissions.
- Since conventional solar stills include a closed chamber, freshwater production occurs only when there is solar radiation. In this design, however, since humid air can flow into the humidification chamber even if there is no radiation (cloudy sky or nighttime), the humid air flows through the humidifier and into the condenser and is finally condensed and freshwater is produced.
- The GHE employed in this research is an EAHE type for conventional air conditioner which also it is used as a condenser for fresh water production simultaneously.

2. Description of the proposed system performance

The system consists of several primary components such as solar still (as humidifier), GHE (as condenser) which includes tubes buried beneath the ground, air flat-plat solar collector and water flat-plat solar collector. A schematic of the proposed system has been drawn in Fig. 1A.

As it can be observed from Fig. 1A, the inlets of the system are air and water (seawater, saline water, brackish water, and highly hard water) which being preheated in two separate flat-plate solar collectors (air and water solar collectors respectively). Afterward, the cycle's inlet water and air enter the system's solar humidification chamber where heat and mass exchange occurs between the two fluids (the solar humidifier's inlet air and the available water inside it). The air gains heat in the process and its temperature rises along with its humidity. The air whose humidity has increased (state 1), i.e. has reached saturation conditions, is pushed by a fan and directed towards tubes buried underground (as condenser) where condensation occurs through heat exchange between tubes and the surrounding soil and humid air's contact with the cold surface of the tubes. Finally, the condensed water inside the tubes is used for drinking (state 4) or irrigation purposes (state 5). Furthermore, since the temperature of the condenser's outlet air (state 3) is the same as that of tubes' surface (ground temperature at the depth in which condensing tubes are buried) and has a relatively constant temperature throughout the year, this air flow can be used in combination with solar PV (state 7) and HVAC (state 6) systems to boost their productivity and also reduce CO_2 emission. A summary of how the proposed system's components are linked together is presented as flowchart in Fig. 1B.

3. Problem statement and formulation

The overall details of the computational model for each part of the desalination unit are formulated based on thermodynamic laws and the principle of mass and heat conservation. The primary hypotheses used for developing the computational model are proposed as follow.

1. Heat and mass loss by the system's components to the surrounding environment is ignored.
2. Air and vapor are considered as perfect gases.
3. The humidifier's outlet air is assumed to be in saturation conditions.
4. Variations in kinetic and potential energy are relatively negligible.

The proposed system's processes may have the following characteristics:

- Air and water flow cycles may be open or closed.
- Energy required for heating air and water may be provided by solar collectors, vapor flow processes and other forms of renewable energies as well as solar humidifier's surface.
- Buried condenser's outlet air may flow back into the solar humidifier before complete drying to reduce the condenser' surface.

Thermodynamic and mass and energy conservation equations are written for each part of the system and the proposed system's computational and mathematical models are obtained. Finally, equations are solved by MATLAB software and results are analyzed.

3.1. Ground heat exchanger (GHE)/Earth air heat exchanger (EAHE)

GHE is one of the crucial units of a solar humidification-dehumidification system. The most common type of condensation in this unit is surface condensation in which cold walls have a lower temperature than the humid air's local saturation temperature. Fig. 2 provides a schematic view of the subsurface condenser's chamber. Saturation air flows into the ground heat exchanger where its temperature falls down due to heat transfer at the isothermal level inside the tube buried beneath the soil and its humidity condenses. The water produced in this system is collected as freshwater for drinking or for direct irrigation of tree roots. The air flowing out of the underground heat exchanger which has almost the same temperature as ground is utilized in other systems for cooling or heating.

Considering the control volume selected in Fig. 2, the equation for heat exchange between air and underground tube's wall surface is solved using Eq. (1) [39].

$$q_{cond} = Lh_m(\varphi\rho_{v,s}(T_a) - \rho_{v,s}(T_p)) \quad (1)$$

In the above equation L, q_{cond}, φ, $\rho_{v,s}(T_a)$, and $\rho_{v,s}(T_a)$ respectively denote tube length, condensation heat transfer, relative humidity, saturation vapor density at air temperature and saturation vapor density at tube's permanent temperature. h_m is convection heat transfer coefficient which is obtained from Eq. (2) [40].

$$h_m = Sh_D\frac{D_{AB}}{D} \quad (2)$$

where, Sh_D is Sherwood number for the developed laminar flow inside the tube $Sh_D = 3.66$ [46]; D_{AB} is the binary diffusion coefficient which, based on the developed equation by Bolz and Tuve [41] is equal to Eq. (4).

$$Sh_D = 3.66 \quad (3)$$

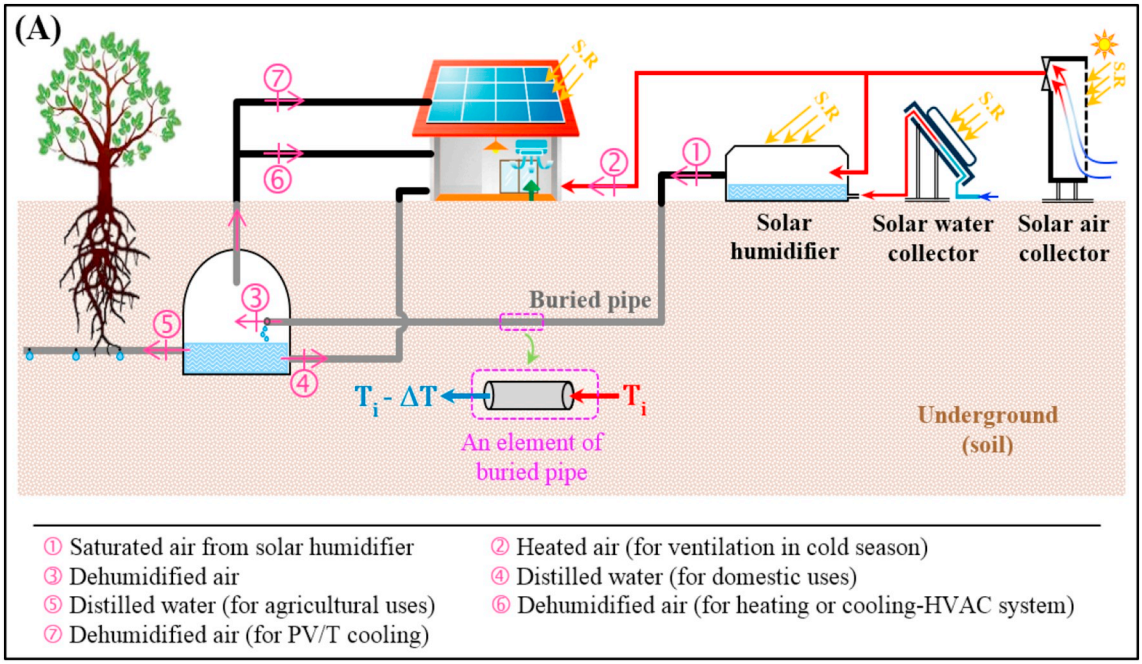

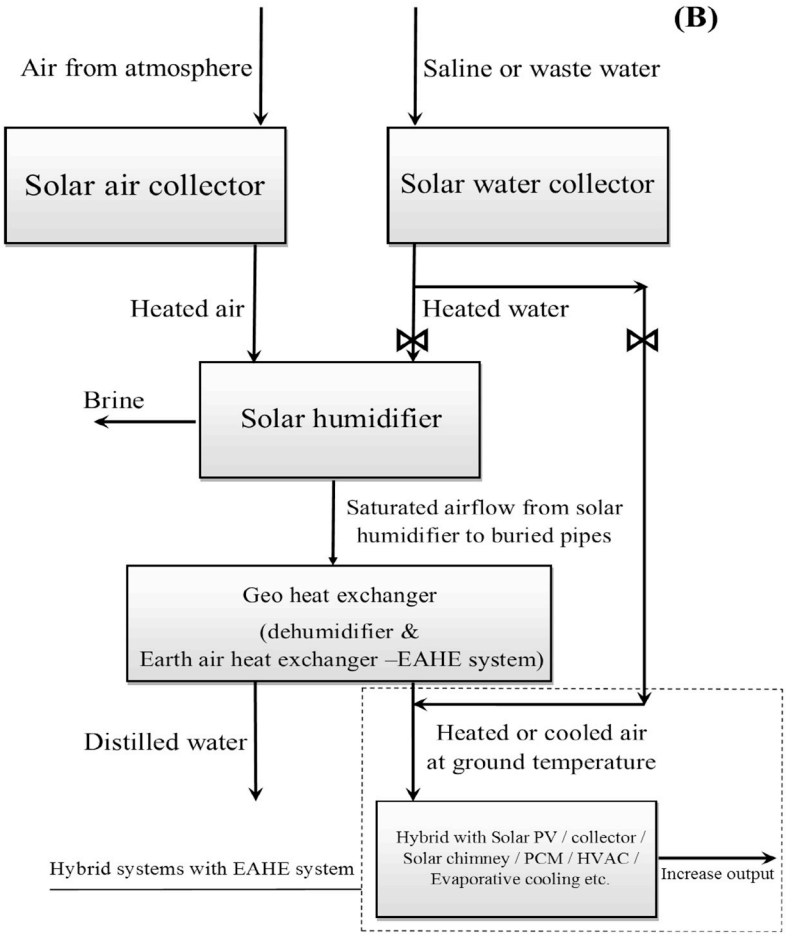

Fig. 1. A schematic of the, (A) proposed system, (B) connection between system components.

$$D_{AB} = -2.775 \times (10^{-6}) + 4.479 \times (10^{-8})T + 1.65610^{-10}T^2 \quad (4)$$

By calculating heat transfer between the air and buried tube's wall, the volume of condensed water is obtained from the following equation [39].

$$\dot{m}_c = \pi D \Delta z \frac{q_{cond}}{L} \quad (5)$$

where, D and Δz are, respectively, diameter of the condenser tube and spacing between the tubes which is 1. Taking into account condensed

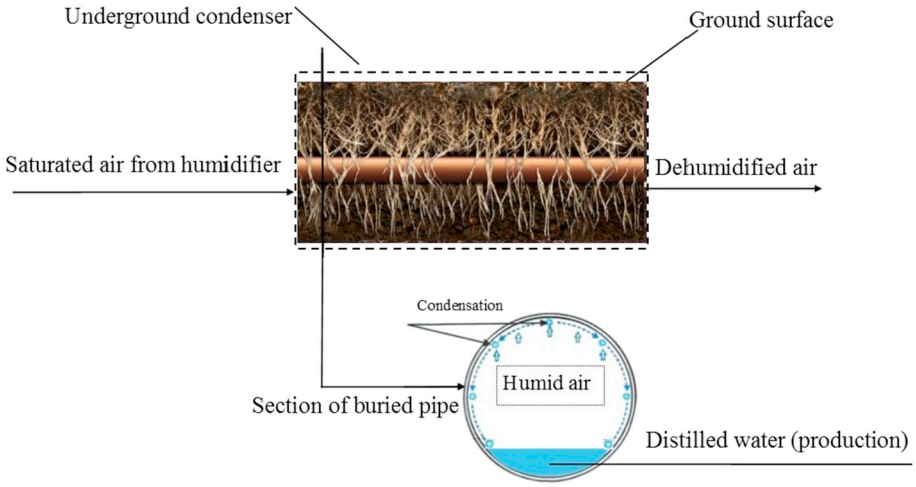

Fig. 2. A schematic of condenser/Geo heat exchanger.

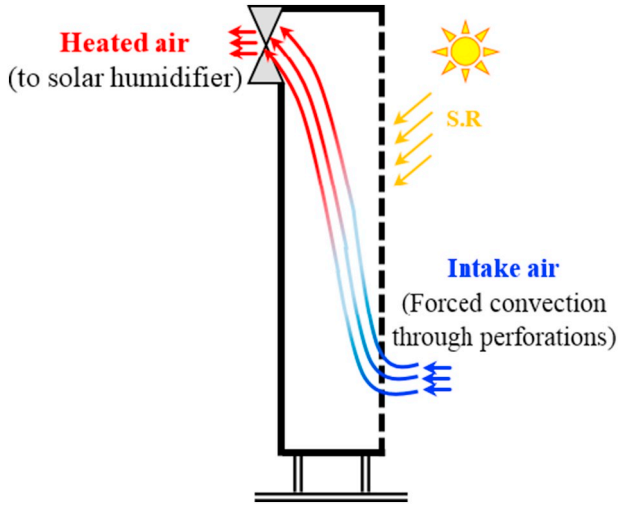

Fig. 3. A schematic of solar air collector.

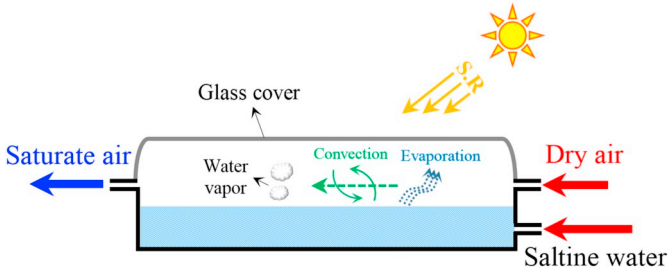

Fig. 4. A schema of solar humidifier unit.

water's mass and mass balance for air control volume, specific humidity for each control volume will be obtained from the following equation.

$$w_{i+1} = w_i - \frac{\dot{m}_c}{\dot{m}_a} \tag{6}$$

3.2. Flat-plate solar collector (air & water)

A schematic of the flat-palate air solar collector is drawn in Fig. 3. In this section, the equations pertaining to the flat-plate solar collector used for increasing the temperature of the solar humidifier's inlet water and air are provided. The energy absorbed by the fluid from the collector is given in the following equation [42].

$$q_{u,water} = \dot{m}_{water} C_{p,water} (T_o - T_i) \tag{7}$$

According to the following equation, known as Hottel-Whillier equation [43], taking into account solar collector's heat losses to the atmosphere, the amount of useful heat obtained from the flat-plate solar collector will be:

$$q_u = A_c [G_t \tau\alpha - U_L (T_P - T_a)] \tag{8}$$

By taking into account Eqs. (7) and (8), the temperature of flat-plate solar collector's outlet water is obtainable from the equation below.

$$T_o = \frac{A_c [G_t \tau\alpha - U_L (T_P - T_a)]}{\dot{m} C_p} + T_i \tag{9}$$

In this equation, U_L is the total heat loss coefficient for the flat-plate solar collector provided by the following equation [44].

$$U_L = \frac{Q_T + Q_B + Q_E}{A(T_p - T_a)} \tag{10}$$

in which, the parameters Q_T, Q_B and Q_E are rate the rate of energy loss due to edge effects, the rate of energy conducted through the bottom insulation and the rate of energy lost by radiation and convection to the glass covers above, respectively. These parameters can be determined using Eqs. (11) to (18).

Tabor defines parameter Q_T in Eq. (10) as [45]:

$$Q_T = \frac{(T_P - T_a)A}{\frac{N}{(C/T_P)[(T_P - T_a)/(N+f)]^{0.33}} + \frac{1}{h_w}} + \frac{\sigma(T_P^4 - T_a^4)A}{\frac{1}{\varepsilon_P + 0.05N(1-\varepsilon_p)} + \frac{2N+f-1}{\varepsilon_g} - N} \tag{11}$$

In this equation, parameters C, f and h_w are defined as [45]:

$$f = (1 - 0.04h_w + 0.0005h_w^2)(1 + 0.091N) \tag{12}$$

$$C = 365.9(1 - 0.00883s + 0.0001298s^2) \tag{13}$$

$$h_w = 5.7 + 3.8W \tag{14}$$

In Eq. (10), we have parameter Q_B which is proposed as Eq. (15) by Tabor [45].

$$Q_B = A(T_P - T_a)/(\delta/k + 1/h_b) \tag{15}$$

As Eq. (15) defines, Q_B depends on width (δ) and heat conduction coefficient (k) of the solar absorptive heat insulator and also to the convection heat transfer coefficient between the insulator and surroundings (h_b). According to the report by Tabor, h_b is equal to [45]:

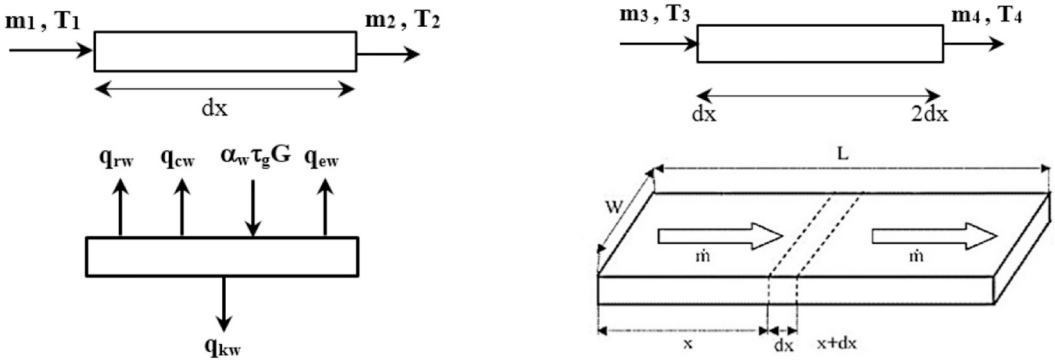

Fig. 5. Schematic of water control volume in solar humidifier.

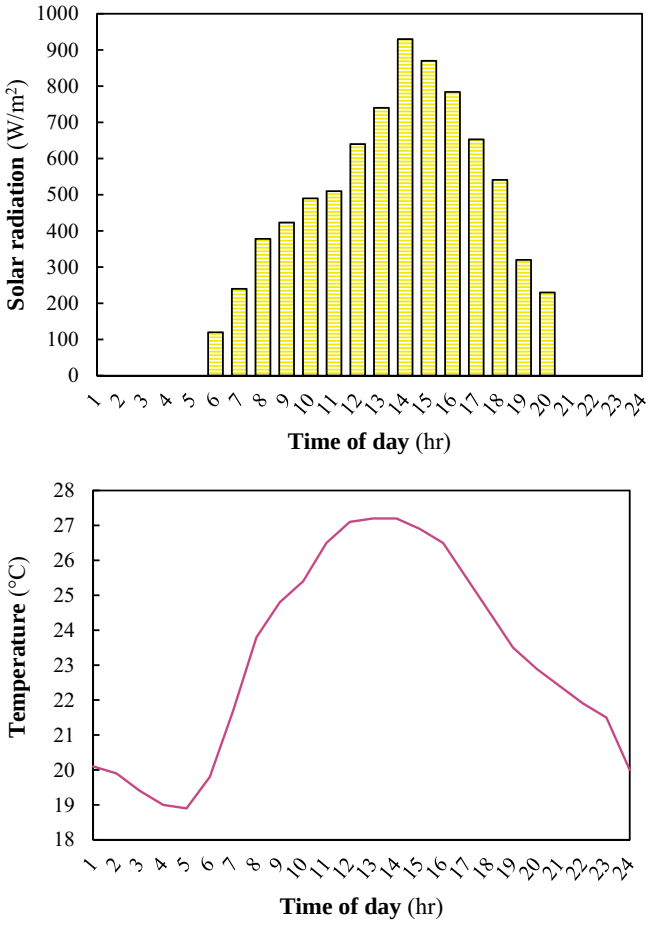

Fig. 6. (up) Variations of solar radiation intensity, (down) Variations in the inflow air temperature of solar air collector.

$$h_b \cong 12.5 \text{ to } 25\ (Wm^{-2}K^{-1}) \tag{16}$$

Another parameter in Eq. (10) is Q_E which, according to the study by Whillier [46], is defined as Eq. (17).

$$Q_E = h_e A_P (T_P - T_a) \tag{17}$$

$$h_e \cong 0.5\frac{W}{m^2K} \tag{18}$$

In the present research, an unglazed solar air collector with perforated absorbent plate is employed to increase the temperature of the system's inlet air. One of the advantages of using this type of collector is that it is installable and applicable in different horizontal to vertical angles. This enables us to install on it building walls, hence reduce its weight and the installation costs. The air leaving this solar collector (which is has the same temperature as the solar humidifier's inlet air) is obtained from the following equations [47,48].

$$Q_{the} = Q_{abs} - Q_{losses} = h_{the}(T_p - T_{out}) \tag{19}$$

$$T_{out} = T_p - \frac{Q_{the}}{h_{the}} \tag{20}$$

The h_{the} inside the solar air collector is obtained from the following equation [47,49].

$$h_{the} = \frac{Nu_{the}K_{air}}{D_h},\ Nu_{the} = 0.0158(Re)^{0.8}$$
$$K_{air} = (0.0015215 + 0.097459T - 3.3322 \times 10^{-5}T^2) \times 10^{-3} \tag{21}$$

The collector's heat absorption, Q_{abs}, is obtained from Eq. (22) [48].

$$Q_{abs} = I_b F_t A_c \tag{22}$$

$$F_t = \alpha_p F_{sh} F_d \tag{23}$$

The collector's heat loss is denoted by Q_{losses} [48].

$$Q_{losses} = U_T A_c (T_p - T_{in}) \tag{24}$$

The collector's overall heat transfer coefficient is denoted by U_T as calculated by Duffie and Beckman [48].

Table 1
Initial inlet parameters.

Height of water existing in humidifier (m)	Temperature of inlet water (°C)	Condensation temperature (°C) 18/October/2017
0.009	27	19
Air velocity (m/s)	**Width of solar humidifier (m)**	**Inflowing air cross-section (m^2)**
0.1	1	0.1

Table 2
Comparison of the amount of vaporized water and water temperature in the humidifier during a day between the present work and Sartori [56].

Parameters	Studies	Time of day (hr)										
		0 AM–2 AM	2 AM–4 AM	4 AM–6 AM	6 AM–8 AM	8 AM–10 AM	10 AM–12 PM	12 PM–14 PM	14 PM–16 PM	16 PM–18 PM	18 PM–20 PM	20 PM–22 PM	22 PM–24 AM
Water vaporized in humidifier during a day (kg/m^{2}hr)	Sartori [56]	0.06	0.05	0.05	0.04	0.1	0.42	0.64	0.6	0.42	0.22	0.18	0.16
	Present study	0.08	0.07	0.07	0.0.6	0.05	0.16	0.5	0.68	0.62	0.54	0.42	0.34
Humidifier water temperature fluctuations during a day (°C)	Sartori [56]	27	25	24	24	35	58	63	66	53	39	34	29
	Present study	27	26	26	25	25	34	55	62	66	56	49	43

Table 3
Comparison between results from the present study and that of Lindblom et al. [39].

Parameter	Reference study [39]	Present study
Temperature (°C)	60	60
Relative humidity (%)	70	70
Tube diameter (m)	0.2	0.2
Production (kg/m.day)	2.30	2.43

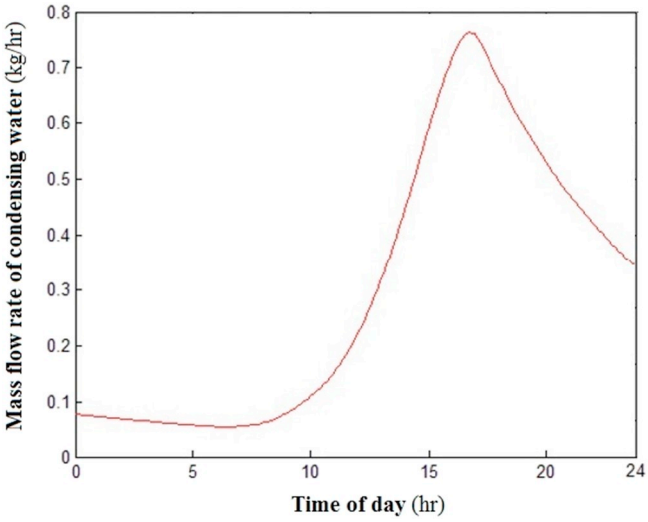

Fig. 7. Variations in freshwater production during the day time.

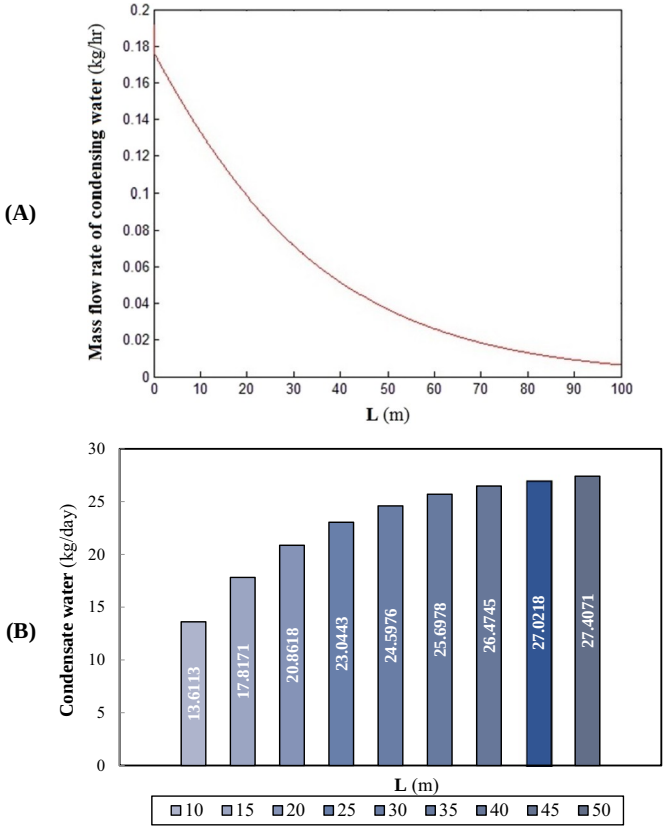

Fig. 8. Variations in freshwater collection throughout the underground tube.

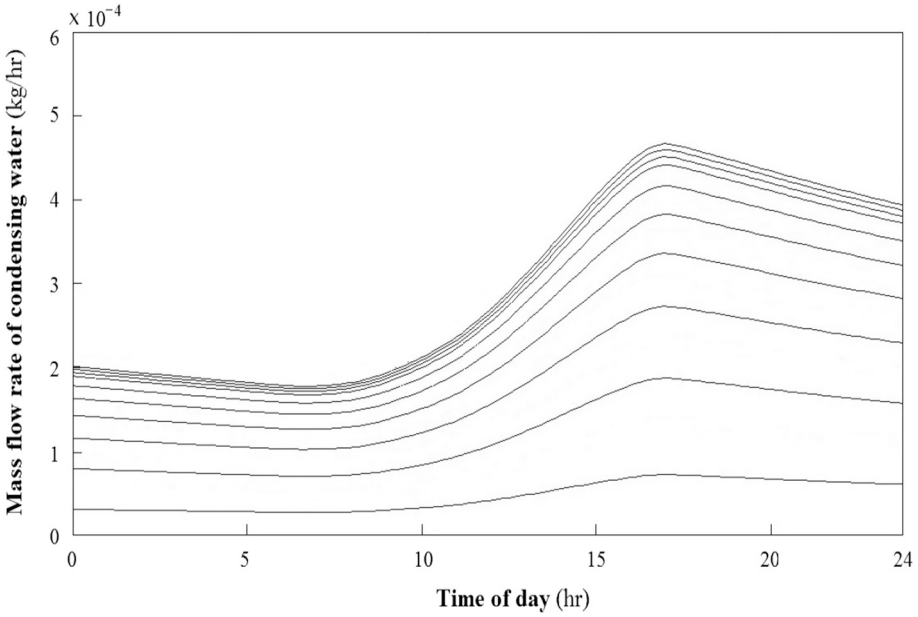

Fig. 9. Variations in condensed freshwater during the day time at different lengths of the underground condenser.

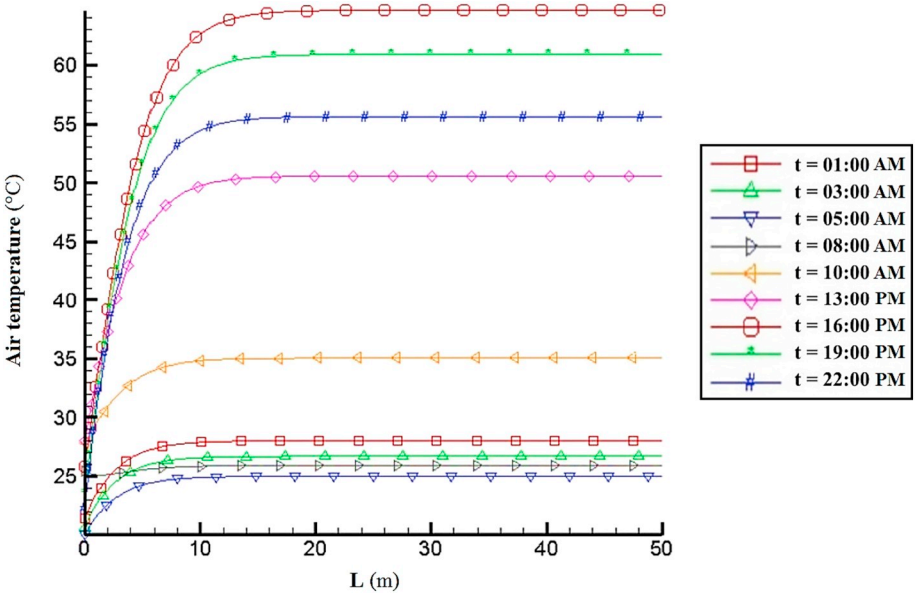

Fig. 10. Air temperature variations throughout the Solar humidifier during the day time.

$$U_T = U_f + U_s + U_b \tag{25}$$

The value of heat transfer coefficient on the rear side of the collector could be determined using Eq. (26).

$$U_b = k_{ins}\frac{A_b}{L} \tag{26}$$

Heat transfer coefficient on collector's walls is obtained from the following equation.

$$U_s = K_{ins}\frac{A_s}{L} \tag{27}$$

Finally, heat transfer coefficient on the frontal side of the system, U_f, can be derived from Klien's empirical equation [45,48].

$$U_f = \left[\frac{M}{\left[\left(\frac{344}{T_p}\right)\left(\frac{(T_p - T_{air})}{(M+(1-0.04h_w+0.0005h_w^2)(1+0.091M))}\right)\right]} + \frac{1}{h_w}\right]^{-1} + \left[\frac{\sigma(T_p - T_{air})(T_p^2 - T_{air}^2)}{[\varepsilon_p + 0.0425M(1-\varepsilon_p)]^{-1} + \left[\frac{2M+f-1}{\varepsilon_g}\right] - M}\right] \tag{28}$$

The parameter h_w is determined using Eq. (14).

3.3. Solar humidifier

After writing flat-plate solar collector's equations, equations related to solar humidification unit, which is responsible for increasing the

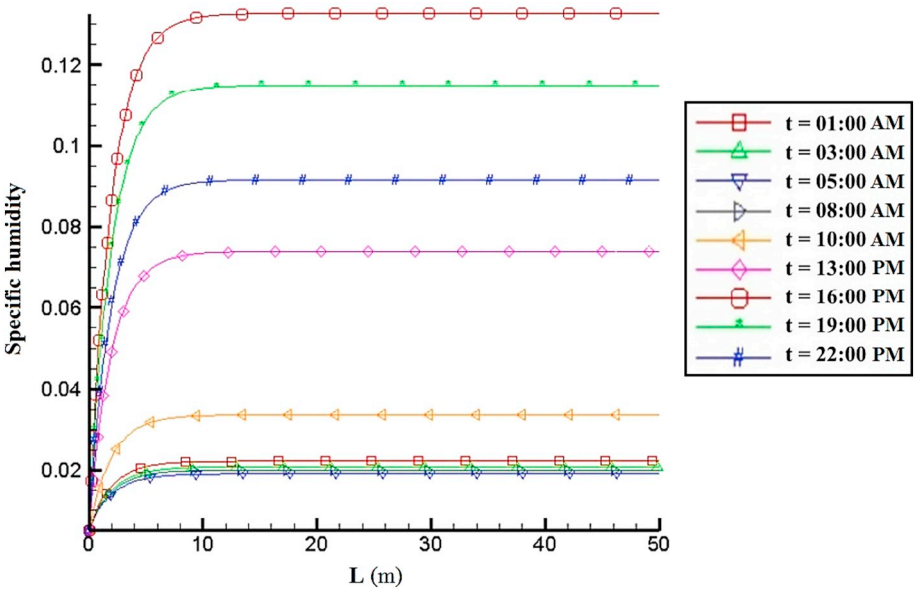

Fig. 11. Variations in air's specific humidity through the solar humidifier during the day time.

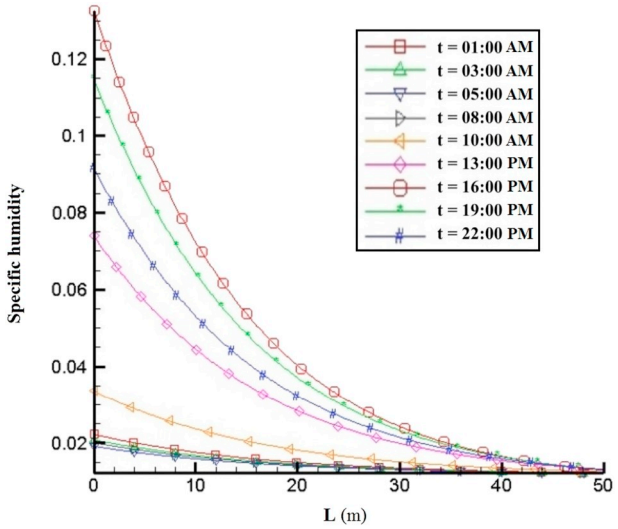

Fig. 12. Variations in air's specific humidity throughout the underground condenser tube during the day time.

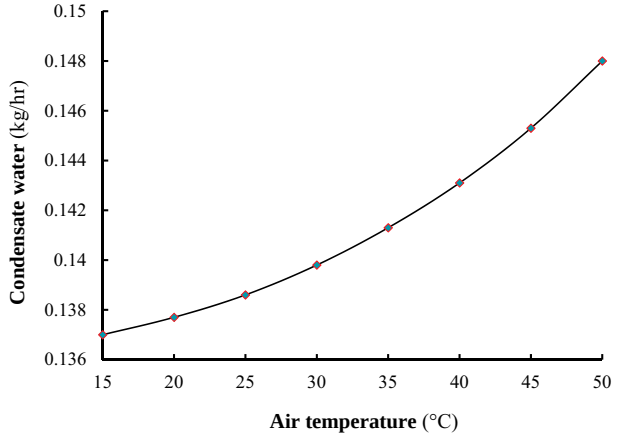

Fig. 13. Effect of solar collector's outlet air on the mass flow rate of the produced freshwater.

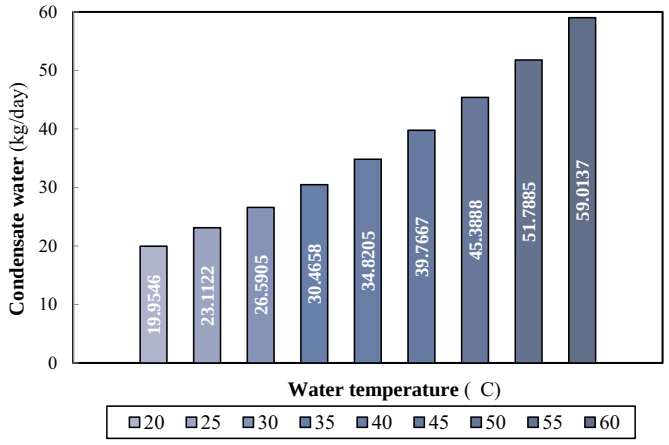

Fig. 14. Effect of solar collector's outlet water temperature on freshwater production.

ratio of outlet humidity to inlet humidity as well as increasing the unit's outlet air temperature, are written.

The air flowing over water surface is divided into elements with lengths of *dx*; the air passes over this element through a duration of *dt*. The amount of time it takes for the air to flow through the humidifier until it reaches saturation is Δ*t*. The temperature of water in the humidifier is assumed to be constant throughout the duration of air passing through the humidifier and reaching saturation conditions. Once the air reaches the end of its path after a time interval of Δ*t*, water's new temperature is obtained by solving energy balance equation for the total water existing in the solar humidifier. Thus, in order to obtain the temperature of the solar humidifier's outlet air as shown in Fig. 4, mass and energy balance equations are derived as presented below. The first law of thermodynamics is initially written for a small control volume with a length of *dx* for air [50].

$$\dot{Q}_{c.v} + \sum \dot{m}_i h_i = \sum \dot{m}_o h_o \tag{29}$$

$$(\dot{m}_a h_{ao} + \dot{m}_{vo} h_{vo}) - (\dot{m}_a h_{ai} + \dot{m}_{vi} h_{vi}) = q_{cw} + q_{ew} \tag{30}$$

where $\dot{Q}_{c.v}$, $\dot{m}$, h, q_{ew}, and q_{cw} are rate of cycle's heat gain, flow rate, enthalpy, vaporization heat transfer and convection heat transfer, respectively. In addition, subscripts i, o, a, and v denote inlet flow, outlet

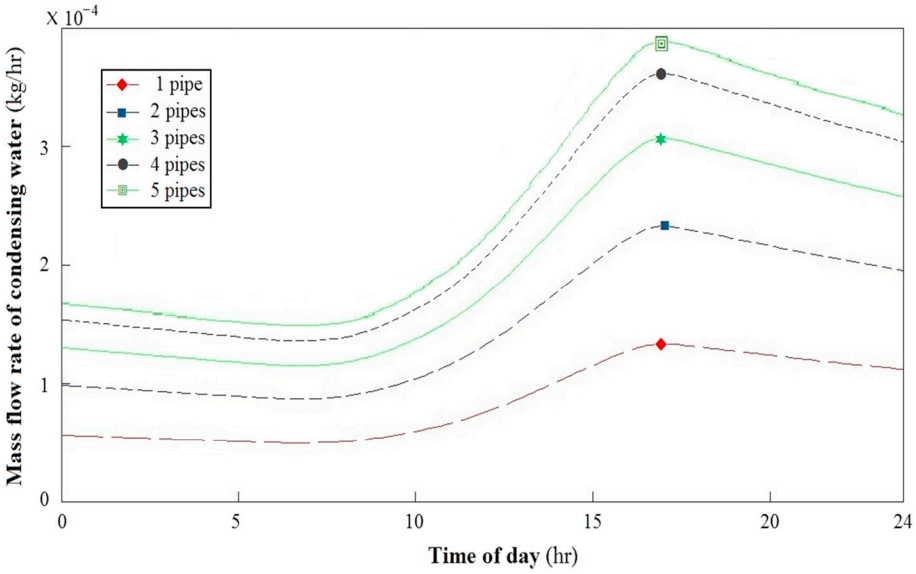

Fig. 15. Effect of tube numbers on freshwater production rate.

flow, dry air and water vapor, respectively. Humidity ratio is defined by $\omega_i = m_{v,\,i}/m_a$ [50].

Dividing Eq. (30) by $\dot{m}_a$ gives:

$$h_{ao} + \omega_o h_{vo} - h_{ai} - \omega_i h_{vi} = \frac{1}{\dot{m}_a}(q_{cw} + q_{ew}) \tag{31}$$

$$c_{pa}(T_{o,h} - T_{i,h}) + \omega_o h_{vo} - \omega_i h_{vi} = \frac{1}{\dot{m}_a}(q_{cw} + q_{ew}) \tag{32}$$

In Eq. (32), the degree of the temperature entering the solar humidifier, $T_{i,\,h}$, is equal to the temperature of the air discharged from the flat plate solar collector obtained by Eq. (33).

$$T_{i,h} = T_p - \frac{I_b F_t A_c - U_T A_c (T_p - T_{in})}{\frac{Nu_{the} K_{air}}{D_h}} \tag{33}$$

where ω and c_{pa} respectively are specific humidity and specific heat at constant pressure for air. Vapor enthalpy in the thermal range of $-10\,^{\circ}C < T < 50\,^{\circ}C$ can also be derived from the following equation with marginal error [51].

$$h_g(T) = 2501.3 + 1.82T,\ h_v \cong h_g \tag{34}$$

In the above equation, h_g is vapor enthalpy at saturation conditions. Therefore, by substituting Eq. (33) in Eq. (32), Eq. (35) is obtained.

$$c_{pa}\left(T_{o,h} - T_p + \frac{I_b F_t A_c - U_T A_c (T_p - T_{in})}{\frac{Nu_{the} K_{air}}{D_h}}\right) + \omega_o h_{vo} - \omega_i h_{vi} = \frac{1}{\dot{m}_a}(q_{cw} + q_{ew}) \tag{35}$$

In the equation above, temperature is in centigrade. In balance equation of the first thermodynamics law, Eq. (35), the goal is to obtain ω_o and T_{ao}. Furthermore, in Eq. (35), q_{ew} represents rate of vaporization heat transfer between water and air which is defined as follows [52]:

$$q_{ew} = \left(\frac{h_c}{C_{p,air}}\right) L_w (X_s - X_n) A \tag{36}$$

where h_c, L_w and X_s denote forced convection heat transfer coefficient, latent heat of water vaporization and saturation air's specific heat at the temperature of humidifier water, respectively, which are obtained from Eqs. (37)–(39) [52,53]. Also, $C_{p,\,air} = 1005$ J/kgK is air's specific heat (with a constant value), X_n is the specific humidity of the air in the humidifier (with a given value) and A is the humidifier's cross-section.

$$h_c = 2.8 + 3V \tag{37}$$

$$L_w = 2500.8 - 2.36T + 0.0016T^2 - 0.00006T^3 \tag{38}$$

$$X_s = \frac{P_{ws}}{P_{tot}} \times \frac{M_w}{M_a} \tag{39}$$

In Eq. (38), T is water temperature in centigrade. In Eq. (39), P_{ws} is the pressure of saturation air at humidifier's water temperature which is can be derived from thermodynamic tables. In addition, V, P_{tot}, M_w, and M_a in the above equations respectively represent velocity of inlet air into the cycle, total pressure, and water and air's molar mass.

Convection heat transfer between water and the air flowing over it is calculated using Eq. (40) [52]:

$$q_{cw} = h_c A(\Delta T) \tag{40}$$

where ΔT is thermal difference between water and air.

Using mass balance, the specific heat of the air leaving each element is calculated by the following equation.

$$\omega_o = \omega_i + \frac{g_s}{\dot{m}_a} \tag{41}$$

Mass of vaporized water, g_s, is calculated by Eq. (42) [52].

$$g_s = \left(\frac{h_c}{C_{p,air}}\right)(X_s - X_n)A \tag{42}$$

By solving Eqs. (35)–(42), temperature of the air leaving each element through the humidifier is calculated and as a result, temperature in the system's transient problem will be obtained.

After writing the equations pertaining to energy balance for glass, glass temperature will be calculate using the following equation derived from references [54, 55].

$$T_g = \frac{(0.02612T_w^2 - 15.76T_w + 2392)T_w + A_r h_w T_a + A_r(0.048T_a - 9)T_s}{(0.02612T_w^2 - 15.76T_w + 2392) + A_r h_w + A_r(0.048T_a - 9)} \tag{43}$$

In the above equation, T_g, T_w, A_r and h_w respectively denote glass temperature, temperature of water in the humidifier's chamber, ratio of glass surface to solar humidifier's bottom surface and forced air convection coefficient.

T_s is sky temperature and is obtained by the following equation

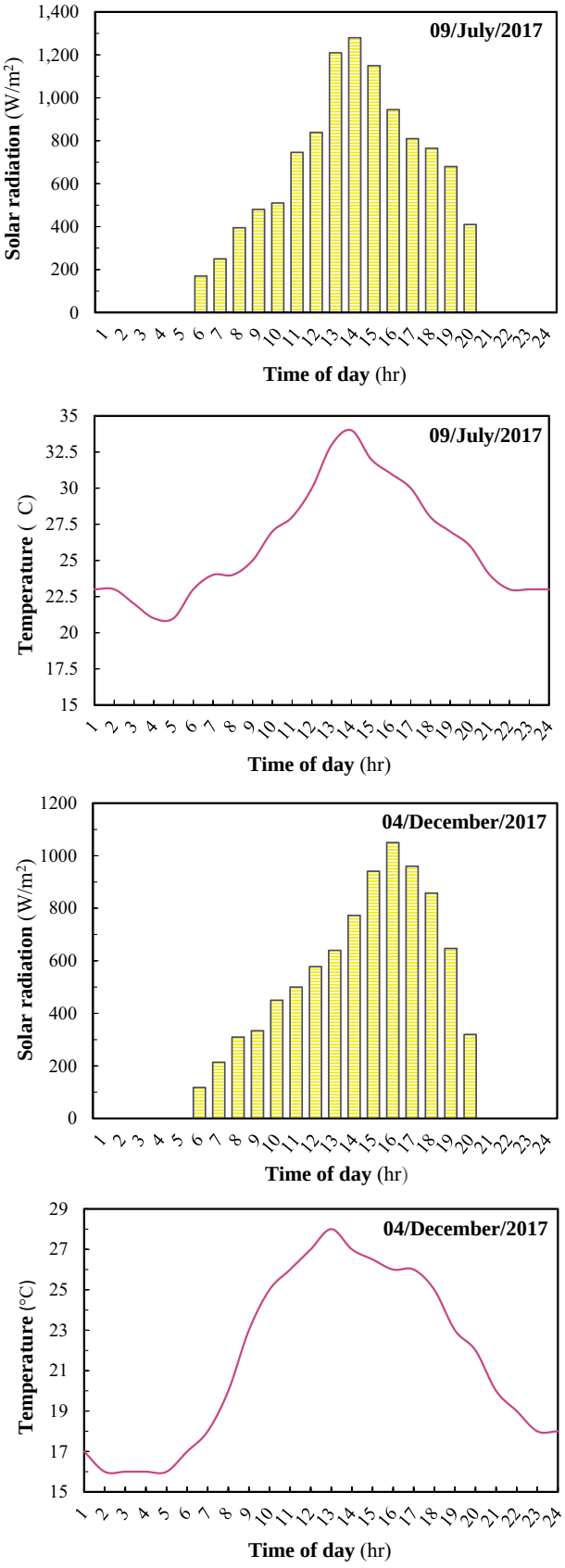

Fig. 16. Variations of solar radiation intensity and inflow air temperature of solar air collector for 9th July and 4th December 2017.

using the ambient temperature [55].

$$T_s = 0.0552 T_a^{1.5} \tag{44}$$

After calculating glass temperature as well as humid air's characteristics through the entire length of the solar humidifier, energy balance is written for the humidifier's entire chamber and by solving it, the temperature of water in the solar humidifier after ΔT time is calculated. Energy balance equation for water control volume is formulated by Eq. (45) [56].

$$\frac{c_w}{A}\frac{dT_w}{dt} = \alpha_w \tau_g G - q_{cw} - q_{rw} - q_{ew} - q_{kw} \tag{45}$$

In other words,

$$\frac{c_w}{A}\frac{T_w^{K+1} - T_w^K}{\Delta t} = \alpha_w \tau_g G - q_{cw} - q_{rw} - q_{ew} - q_{kw} \tag{46}$$

$$T_w^k = T_o = \frac{A_c\,[G_t \tau\alpha - U_L(T_P - T_a)]}{\dot{m} C_p} + T_i \tag{47}$$

In Eq. (46), c_w, $T_w{}^{K+1}$, $T_w{}^K$, Δt, α_w, τ_g and G represent heat capacity of water, temperature of water at new time, initial temperature of water, time interval, water absorption coefficient, glass emissivity coefficient and degree of irradiance, respectively. And q_{rw} and q_{kw} are respectively, emittance heat transfer between water and glass and heat transfer between water and the surrounding area of the humidifier which are calculated by Eqs. (48) and (49) [56].

$$q_{rw} = 0.9\sigma(T_w^4 - T_g^4) \tag{48}$$

$$q_{kw} = k_{bs}(T_w - T_a) \tag{49}$$

In the above equation, σ is Stefan–Boltzmann constant and k_{bs} is coefficient for solar humidifier's total heat transfer to the surroundings. The unknown variable of Eq. (46) is water temperature which is obtained for dt time by solving the equation. At this time, the air has reached the length of dx. After another dt interval and air's progress through the chamber until $2dx$, water temperature at $2dt$ is calculated. Therefore, the first law is written once for control volume for the distance between zero and dx and once more for the distance between dx and $2dx$. Fig. 5 shows the air's two consecutive control volumes of equal lengths.

The parameter of m_3 in the above figure is equal to m_2 in the previous element. By solving the first law for the two given control volumes, temperatures T_2 and T_4 are obtained. As a result, temperature of water at time $2dt$ is calculated using energy balance for water. This process continues for the remaining length of the chamber and water temperature and specific humidity of air as well as air temperature are obtained for different intervals and spacing in the solar humidifier. This will result in transient problem solution.

3.4. Inlet parameters of the cycle

Solar irradiance measured using a solarmeter. Using these data and after making sure about that validity of the equations and the proposed computational model, equations are solved in MATLAB software and results are obtained. The cycle's given inlet parameters are provided in Fig. 6 and in Table 1. The data are registered by the Meteorological Organization of the City of Chabahar for 18 October of 2017.

4. Validation of numerical results

The aim of this section is to validate the results of numerical simulation. To achieve this goal, the temperature of the water in the solar humidifier and the amount of vaporized water throughout the day in

Table 4
Initial inlet parameters for 9th July and 4th December 2017.

Wind speed (m/s) 09/July/2017	Wind speed (m/s) 04/December/2017	Temperature of inlet water (°C)	Height of water existing in humidifier (m)
9	12	27	0.09

Width of solar humidifier (m)	Air velocity (m/s)	Inflowing air cross-section (m^2)
1	0.1	0.1

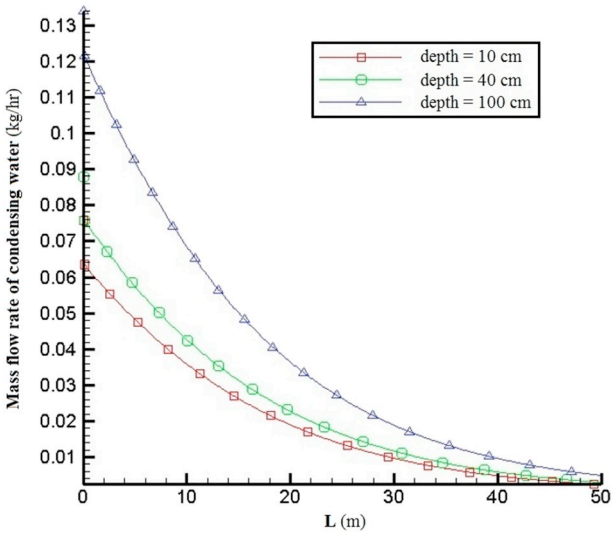

Fig. 17. Variations in freshwater throughout the tube by altering the underground condenser depth (14:00 PM (09/July/2017)).

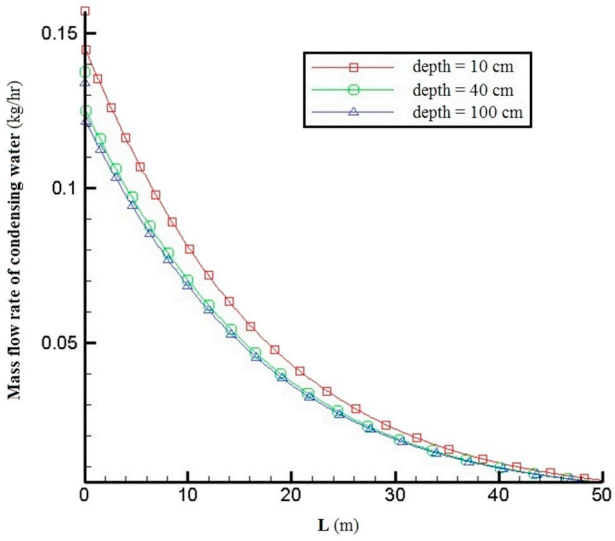

Fig. 18. Variations in freshwater throughout the tube by altering the underground condenser depth (04:00 AM (04/December/2017)).

the present research are compared with the experimental results of Sartori [56] in Table 2. The increase in water temperature and mass of vaporized water as well as the changes in these two quantities throughout the day are similar in both and the negligible variation in the comparison of the results indicates the validity of the results from the present numerical analysis.

In order to find the thermodynamic conditions for each part of the cycle as well as to predict freshwater production rate, the governing equations solved simultaneously. In order to validate the numerical results, Table 3 compares results from the present research and those of Lindblom et al. [39].

5. Results and discussion

5.1. Analyzing specifications of the proposed system

The aim of writing the computational code was to obtain the system's freshwater output based on given inlet parameters including flat-plate solar collector's inlet air's temperature at different times of the day, inlet air's humidity and debit, degree of solar irradiance at different hours of the day, solar humidifier and flat-plate solar collector's inlet water temperature, and temperature of the earth in the depth at which condenser tubes are buried. At first, the system itself was assessed which only consisted of a solar still as solar humidifier and a subsurface condenser (as dehumidifier). By solving equations and evaluating the parameters affecting the system by Design-Expert software (DOE), the impact of the cycle's inlet water temperature was evaluated. The evaluation revealed that an increase in temperature of the water flowing into the humidifier from 25 to 42° centigrade increases freshwater production in the system by 25% [38].

Considering the DOE analysis of the system we may conclude that increased inlet water and air temperature has a relatively significant effect on the system's freshwater output. Therefore, the effect of using solar water collector as well as solar air collector is evaluated for this cycle. In addition, it worth noting again that using solar collectors reduces energy consumption in other cycles under study in this system.

After solving the system's thermodynamic equations, variations in the system's freshwater production throughout a 24-hour period are derived and presented in Fig. 7. As Fig. 7 shows, freshwater production reaches its maximum at the peak hours of solar radiation and inlet air temperature and then decreases with them. As a result, similar to the trend of variations in the diagrams related to solar irradiance and ambient air temperature, freshwater production reaches its highest level throughout the day at the peak hours of solar radiation.

Table 5
Variations in freshwater by altering the underground condenser depth (14:00 PM (09/July/2017)).

Mass of distilled water (kg/hr)	Ground temperature (°C)	Underground condenser depth (cm)	Relative humidity (%)	Solar radiation (W/m^2)
10.02	34	5	64	1280
11.98	28	40	64	1280
19.24	21	100	64	1280

Table 6
Variations in freshwater by altering the underground condenser depth (04:00 AM (04/December/2017)).

Mass of distilled water (kg/hr)	Ground temperature (°C)	Underground condenser depth (cm)	Relative humidity (%)	Solar radiation (W/m^2)
22.79	17	10	91	0
19.78	19	40	91	0
18.24	20	100	91	0

Table 7
Fixed costs related to the proposed system.

Units		Amount	Cost of equipment for one unit (US $)	Total Cost of equipment (US $)
Solar humidifier	Iron sheet (1.5 mm thick)	20 m^2	20	400
	Glass cover	15 m^2	6	90
	Paints and silicon	20 m^2	12	240
	Insulation	20 m^2	5	100
Flat plat collectors and heat exchanger		15 m^2	250	3750
Fan & circulate pump		2. No	25	50
Five aluminum's tube		5 × 50	3 US $ per meter	750
Production		–	100	100
Total fixed costs (*FC*)				5480

Table 8
Cost of production per average daily productivity and Comparison of different desalination system.

Low cost solar stills	Present work	Active still with vacuum fan, [57]	Single basin still coupled to evacuated tube collector, [59]	Stepped solar still with external and internal reflector, [58]
Cost of fresh water production (kg or lit)	0.0276 US $/lit	0.048 US $/lit	0.0186 US $/lit	0.0197 US $/litter

Fig. 8A shows the hourly rate of freshwater production through the condenser tube; as it can be seen, with the decreasing of air humidity through the tube, the amount of freshwater collected reduces.

Fig. 8B shows the amount of freshwater collected at different lengths of the condenser tube throughout a 24-hour period. The total amount of freshwater production through the condenser should naturally increase by moving away from the condenser tube opening, but because the humidity of the air decreases as it flows through the length of the tube, freshwater production has a falling rate. By increasing the condenser's length from 10 to 25 m, production increases from 13.6113 kg/day to 23.0443 kg/day which is an increase of 69.30%. However, increasing the length from 25 to 40 m results in a mere 14.89% production boost which indicates that as the air current flows further in the condenser, it loses its humidity increasingly and as a result, freshwater production decreases and the increasing has a falling rate.

Fig. 9 shows the effect of tube length on freshwater production rate at different hours during a 24-hour period. By increasing tube length, the amount of freshwater collected also increases, but this increase has a descending rate so that for higher lengths, the effect of changing tube length on freshwater production is marginal.

Fig. 10 shows changes in humid air temperature through the solar humidifier at different hours of the 24-hour period. Air temperature is increasing incrementally. Also, similar to changes in the temperature of water in the humidifier, air temperature initially increases and then declines throughout the period. As the figure shows, the humidification chamber length required for the air flowing over water surface to have the same temperature as water is between 10 and 15 m.

In Fig. 11 variations in the specific humidity of the air inside the solar humidifier at different hours of the day are presented. As the air permeates further into the solar humidifier it gains more humidity. The length of the humidifier is chosen so that the outlet air is saturated, as seen in the schema below. As it can be observed, the air is saturated at all times of the period with a 20-m long humidifier. In the next part, the impact of different parameters on the length required to attain saturation outlet air is explored. Needless to say, a shorter humidifier length will reduce the costs and the space required for installation of the solar desalinator.

Fig. 12 displays changes in specific humidity of the air throughout the length of the condenser tube for different hours of a 24-hour period; specific humidity of the air is reduced due the condensation process and humidity loss throughout the condenser tube. Similar to the trend of variations as suggested by the diagrams related to irradiance intake and ambient temperature, specific humidity also reaches its highest level at peak solar radiation hours.

The effect of installing air and water solar collector on freshwater production rate in the system will now be explored. At first, the effect of air solar collector on freshwater production rate in the system will be investigates (Fig. 13). As the diagram suggests, when the temperature of the solar collector's outlet air increases from 15 to 40°C, the amount of freshwater production increases by 4.45%; this increase may indicate that under the conditions of inlet air's relative humidity, the cycle's operational temperature increases with inlet air temperature. Hence, vaporization of water increases in the solar humidifier, and as a result, freshwater production increases in the condenser. This shows that the humidity intake of the air passing through the solar humidifier increases with inlet air temperature and as a result, further approaches saturation conditions and more water can be condensed in the condenser, hence more freshwater production.

Fig. 14 shows the effect of inlet water temperature on freshwater production throughout a day. The temperature of the water in the solar humidifier is the same as the temperature of the flat-plate solar collector's outlet air which is added to the system to boost productivity. Increasing the temperature of the existing water in the solar humidifier increases its outlet air temperature. As a result, vaporized water's mass rises through the humidifier due to the cycle's increased operational temperature which finally leads to more freshwater production. This can be accounted for by the fact that when air temperature rises throughout the solar humidifier, the humidity intake of the air passing through the solar humidifier increases and water vapor approaches saturation conditions at constant humidifier length and as a result, more vapor is condensed in the condenser and increases production.

Results indicate that increasing humidifier's inlet water temperature from 20 to 40°C increases freshwater production from 19.9546 kg/day to 34.8205 kg/day which translates to a 74.46% increase. In addition, by increasing the humidifier's inlet water temperature from 40 to 50degrees centigrade, freshwater production increases from 34.8205 kg/day to 45.3888 kg/day which means a 30.35% increase in production.

Fig. 15 shows the effect of the number condenser tubes on freshwater production rate. As it can be seen, freshwater production increases with the number of tubes. On the other hand, adding further to the number of condenser tubes leads to a falling freshwater production rate.

Since temperature of the earth varies at different depths, changing the depth at which condenser tubes are buried and changing the tube's surrounding temperature (i.e. condensation temperature) will also influence the amount of freshwater collected. This section explores the effect of changing underground depth on freshwater mass in months of December and July of 2017.

The cycle's given inlet parameters for these two specific days are provided in Fig. 16 and in Table 4. The data are registered by the Meteorological Organization of the City of Chabahar for 9th July and 4th December of 2017. Solar irradiance for these two days has also been measured using a solarmeter.

Fig. 17 and Table 5 show the effect of altering the depth at which the condenser is buried at 14:00 PM on 09/July/2017. At this time of the day, due to reduced affectability of various factors in the surroundings such as air temperature and solar radiation, increasing the depth at which the condenser is buried decreases its surficial temperature and remains constant from the depth of 1–1.5 m; thus, the amount of collected freshwater increases because of reduced temperature in the condenser tube surface. According to the results shown in Table 5, the amount of freshwater produced in the condenser at depths of 100 cm and 40 cm from the surface of the ground is 19.24 kg/h and 11.98 kg/h, respectively. This suggests that a reduction in the condenser's surface temperature from 28 °C to 21 °C causes a 60.6% percent increase in production.

Fig. 18 and Table 6 show the effect of ground depth at 04:00 AM on 04/December/2017. At this time, increasing the depth at which the condenser is buried increases ground temperature, and this means that condenser's surface temperature also increases, which in return reduces the amount of freshwater collected.

In fact, when the condenser is buried at a shallower depth, ground temperature and thus, condenser's surficial temperature throughout the day changes with variations in ambient temperature, solar radiation and other factors in the surroundings and eventually changes the amount of freshwater production. From the depth of 100 cm onward, however, ground temperature remains steady throughout the period and is less likely to be affected by circumstantial factors and as a result, freshwater's mass remains constant from this depth onward. Therefore, in regions where there is high air humidity 24 h a day, the cycle is able to produce freshwater even at night when there is zero solar radiation by condensing the humidity in the air. Furthermore, since the condenser's outlet air's temperature is the same as the tube's surface (earth temperature at the depth at which condensing tubes are buried), this air current may be utilized for other applications such as solar PVs, collectors, and HVACs.

5.2. Economic analysis of the proposed system

In this section, the effort has been focused on the economic analysis of the proposed system. The economic analysis is based on the method presented by Kabeel et al. [57]. As expressed in Eq. (50), the total costs (*TC*) consist of fixed costs (*FC*) and variable costs (*VC*). The construction cost for each of the system components is listed in Table 7 and based on this table, the total fixed costs is calculated to be *FC* = 5480 US $. Also, the annual *VC*s is considered to be 30% of *FC* (Eq. (51)) [57].

$$TC = FC + VC \tag{50}$$

$$VC = 0.3 \times FC \tag{51}$$

If the useful life of the proposed system has been considered to be 10 years, then $TC = 5480 + (0.3 \times 10 \times 5480) = 21{,}920$ US $. Considering Fig. 15, the amount of daily fresh water production for a condenser with 5 buried pipes is 230.1 lit. In Chabahar city, it could be considered that there are 345 sunny days on average in a year [31]; consequently, the total amount of fresh water produced in the 10-year useful lifespan of the system could be calculated as following:

- Amount of fresh water production = $230.1 \times 10 \times 345 = 793845$ (lit)
- Cost of fresh water production (lit) = $21920/793845 = 0.027$ $

Since the type of condenser and humidifier employed in this design and the method of their integration are innovations of this design and no similar design has so far been introduced, we cannot provide an accurate economic comparison with other solar desalinator. Nevertheless, with regards to Table 8, the cost of building this system compared to other systems is acceptable.

6. Conclusions

In current investigation, the effort has been paid to propose a novel hybrid system for producing fresh water. By coupling a solar desalination system with a subsurface condenser it may produce freshwater even at night when there is no solar radiation by employing convection heat transfer and superficial vaporization as well as by exploiting high air humidity in some regions of the world. In addition, it may increase freshwater production throughout the day using solar air and water collectors. Because the temperature of the condenser's outflowing air is the same as that of the tube's surface (ground temperature at the depth in which condenser tubes are buried), this air flow may be employed for other applications such as solar PVs, collectors, solar chimneys, PCMs, and HVACs. As the results suggest, the depth at which the condenser tubes are buried can significantly influence production rate at different hours of the day. Findings show that if the condenser is installed at a depth of 100 cm below the ground, the amount of freshwater produced, and ground heat exchanger's outlet air temperature will be the least affected by seasonal and circumstantial factors of the surroundings.

- Reducing the condenser's surficial temperature from 28 °C to 21 °C boosts freshwater production by 60.6%.
- The results reveal that on 04/December/2017, the proposed cycle can be used during the night time (on nights with high humidity in the air entering the cycle) through condensation of humidity in fresh air. The amount of freshwater production at 04:00 AM on this date is equal to 18.24 kg/h for a condenser buried at a depth of 1 m from the ground. This amount is remarkable with a freshwater production of 19.24 kg/h on 09/July/2017 in the summer at 14:00 PM when there is a very good sunlight condition.
- Since the condenser's outlet air temperature is the same as the tube's surface temperature (temperature of the earth at the depth in which condenser tubes are buried which is relatively constant throughout the year at the depth 1 m), this air current may be used in combination with other systems such as solar PVs, collectors, solar chimneys, PCMs, and HVACs among others, to boost their productivity and also reduce CO_2 emission.
- Using a solar collector and increasing the inlet water's temperature from 40 °C to 50°C will increase freshwater production rate from 34.8205 kg/day to 45.3888 kg/day which is a 30.35% increase in production.
- An increase in the temperature of the solar collector's outlet air from 15 °C to 40 °C increases freshwater production by 4.45%. This shows that the more the humidifier's inlet air temperature increases, the

humidity intake of the air passing through the solar humidifier will increase further. Therefore, more water vapor may be condensed hence increased freshwater production.

Appendix A. Supplementary data

Supplementary data to this article can be found online at https://doi.org/10.1016/j.desal.2019.06.011.

References

[1] L. Rizzuti, H.M. Ettouney, A. Cipollina, Solar Desalination for the 21st Century, Springer, 2006.
[2] M. Deymi-Dashtebayaz, A. Ebrahimi-Moghadam, S.I. Pishbin, M. Pourramezan, Investigating the effect of hydrogen injection on natural gas thermo-physical properties with various compositions, Energy 167 (2019) 235–245, https://doi.org/10.1016/j.energy.2018.10.186.
[3] T.W. Bank, Renewable Energy Desalination: An Emerging Solution to Close the Middle East and North Africa's Water Gap, Office of the Publisher, The World Bank, Washington, DC, 2012, https://doi.org/10.1596/978-0-8213-8838-9.
[4] E. Isabel, S. Andrea, Sustainable Water for the Future, 1st ed., vol. Volume 2, Elsevier, 2009.
[5] A. Cipollina, G. Micale, R. Lucio, Seawater Desalination, 1st ed., Springer-Verlag, Berlin Heidelberg, 2009, https://doi.org/10.1007/978-3-642-01150-4.
[6] S. Li, K. Dong, J. Wang, X. Zhang, Long term coupled simulation for ground source heat pump and underground heat exchangers, Energy Build. 106 (2015) 13–22, https://doi.org/10.1016/j.enbuild.2015.05.041.
[7] S.K. Soni, M. Pandey, V.N. Bartaria, Ground coupled heat exchangers: a review and applications, Renew. Sust. Energ. Rev. 47 (2015) 83–92, https://doi.org/10.1016/j.rser.2015.03.014.
[8] M. Benhammou, B. Draoui, Parametric study on thermal performance of earth-to-air heat exchanger used for cooling of buildings, Renew. Sust. Energ. Rev. 44 (2015) 348–355, https://doi.org/10.1016/j.rser.2014.12.030.
[9] A. Ebrahimi-Moghadam, M. Farzaneh-Gord, M. Deymi-Dashtebayaz, Correlations for estimating natural gas leakage from above-ground and buried urban distribution pipelines, J. Nat. Gas Sci. Eng. 34 (2016) 185–196, https://doi.org/10.1016/j.jngse.2016.06.062.
[10] A. Ebrahimi-Moghadam, G.M. Farzaneh, D. Bayaz, M. Deimi, Develop an equation to calculate the amount of gas leakage from buried distribution gas pipelines, Iran. J. Mech. Eng 18 (2016) 64–86.
[11] A. Ebrahimi-Moghadam, M. Farzaneh-Gord, A. Arabkoohsar, A.J. Moghadam, CFD analysis of natural gas emission from damaged pipelines: correlation development for leakage estimation, J. Clean. Prod. 199 (2018) 257–271, https://doi.org/10.1016/j.jclepro.2018.07.127.
[12] J. Lindblom, B. Nordell, Water production by underground condensation of humid air, Desalination 189 (2006) 248–260, https://doi.org/10.1016/j.desal.2005.08.002.
[13] V. Bansal, R. Misra, G. Das Agrawal, J. Mathur, Performance analysis of earth–-pipe–air heat exchanger for summer cooling, Energy Build. 42 (2010) 645–648, https://doi.org/10.1016/j.enbuild.2009.11.001.
[14] V. Bansal, R. Misra, G. Das Agrawal, J. Mathur, Performance analysis of earth–-pipe–air heat exchanger for winter heating, Energy Build. 41 (2009) 1151–1154, https://doi.org/10.1016/j.enbuild.2009.05.010.
[15] L. Ozgener, A review on the experimental and analytical analysis of earth to air heat exchanger (EAHE) systems in Turkey, Renew. Sust. Energ. Rev. 15 (2011) 4483–4490, https://doi.org/10.1016/j.rser.2011.07.103.
[16] F. Ascione, L. Bellia, F. Minichiello, Earth-to-air heat exchangers for Italian climates, Renew. Energy 36 (2011) 2177–2188, https://doi.org/10.1016/j.renene.2011.01.013.
[17] D. Adamovsky, P. Neuberger, R. Adamovsky, Changes in energy and temperature in the ground mass with horizontal heat exchangers—the energy source for heat pumps, Energy Build. 92 (2015) 107–115, https://doi.org/10.1016/j.enbuild.2015.01.052.
[18] A.B.M. Alves, A.L. Schmid, Cooling and heating potential of underground soil according to depth and soil surface treatment in the Brazilian climatic regions, Energy Build. 90 (2015) 41–50, https://doi.org/10.1016/j.enbuild.2014.12.025.
[19] S.K. Soni, M. Pandey, V.N. Bartaria, Hybrid ground coupled heat exchanger systems for space heating/cooling applications: a review, Renew. Sust. Energ. Rev. 60 (2016) 724–738, https://doi.org/10.1016/j.rser.2016.01.125.
[20] S. Sanaye, B. Niroomand, Thermal-economic modeling and optimization of vertical ground-coupled heat pump, Energy Convers. Manag. 50 (2009) 1136–1147, https://doi.org/10.1016/j.enconman.2008.11.014.
[21] J.-S. Jeon, S.-R. Lee, W.-J. Kim, Applicability of thermal response tests in designing standing column well system: a numerical study, Energy 109 (2016) 679–693, https://doi.org/10.1016/j.energy.2016.05.023.
[22] G. Florides, E. Theofanous, I. Iosif-Stylianou, S. Tassou, P. Christodoulides, Z. Zomeni, E. Tsiolakis, S. Kalogirou, V. Messaritis, P. Pouloupatis, G. Panayiotou, Modeling and assessment of the efficiency of horizontal and vertical ground heat exchangers, Energy 58 (2013) 655–663, https://doi.org/10.1016/j.energy.2013.05.053.
[23] W. Yang, S. Zhang, Y. Chen, A dynamic simulation method of ground coupled heat pump system based on borehole heat exchange effectiveness, Energy Build. 77 (2014) 17–27, https://doi.org/10.1016/j.enbuild.2014.03.023.
[24] H. Fujii, K. Nishi, Y. Komaniwa, N. Chou, Numerical modeling of slinky-coil horizontal ground heat exchangers, Geothermics 41 (2012) 55–62, https://doi.org/10.1016/j.geothermics.2011.09.002.
[25] H. Fujii, S. Yamasaki, T. Maehara, T. Ishikami, N. Chou, Numerical simulation and sensitivity study of double-layer slinky-coil horizontal ground heat exchangers, Geothermics 47 (2013) 61–68, https://doi.org/10.1016/j.geothermics.2013.02.006.
[26] Y. Wu, G. Gan, A. Verhoef, P.L. Vidale, R.G. Gonzalez, Experimental measurement and numerical simulation of horizontal-coupled slinky ground source heat exchangers, Appl. Therm. Eng. 30 (2010) 2574–2583, https://doi.org/10.1016/j.applthermaleng.2010.07.008.
[27] A. Ebrahimi-Moghadam, B. Mohseni-Gharyehsafa, M. Farzaneh-Gord, Using artificial neural network and quadratic algorithm for minimizing entropy generation of Al 2 O 3-EG/W nanofluid flow inside parabolic trough solar collector, Renew. Energy 129 (2018) 473–485, https://doi.org/10.1016/j.renene.2018.06.023.
[28] B. Mohseni-Gharyehsafa, A. Ebrahimi-Moghadam, V. Okati, M. Farzaneh-Gord, M.H. Ahmadi, G. Lorenzini, Optimizing flow properties of the different nanofluids inside a circular tube by using entropy generation minimization approach, J. Therm. Anal. Calorim. 135 (2019) 801–811, https://doi.org/10.1007/s10973-018-7276-x.
[29] M. Jannatabadi, M. Farzaneh-Gord, H.R. Rahbari, A. Nersi, Energy and exergy analysis of reciprocating natural gas expansion engine based on valve configurations, Energy 158 (2018) 986–1000, https://doi.org/10.1016/j.energy.2018.06.103.
[30] O.O. Badran, M.M. Abu-Khader, Evaluating thermal performance of a single slope solar still, Heat Mass Transf. 43 (2007) 985–995, https://doi.org/10.1007/s00231-006-0180-0.
[31] V. Okati, S. Farsad, A. Behzadmehr, Numerican analysis of an integrated desalination unit using humidification-dehumidification and subsurface condensation processes, Desalination 433 (2018), https://doi.org/10.1016/j.desal.2017.12.029.
[32] V. Okati, A. Behzadmehr, S. Farsad, Analysis of a solar desalinator (humidification–dehumidification cycle) including a compound system consisting of a solar humidifier and subsurface condenser using DoE, Desalination. 397 (2016) 9–21, https://doi.org/10.1016/j.desal.2016.06.010.
[33] S.A. Nada, H.F. Elattar, A. Fouda, Experimental study for hybrid humidification–dehumidification water desalination and air conditioning system, Desalination 363 (2015) 112–125, https://doi.org/10.1016/j.desal.2015.01.032.
[34] A. Fouda, S.A. Nada, H.F. Elattar, An integrated a/C and HDH water desalination system assisted by solar energy: transient analysis and economical study, Appl. Therm. Eng. 108 (2016) 1320–1335, https://doi.org/10.1016/j.applthermaleng.2016.08.026.
[35] S.A. Nada, H.F. Elattar, A. Fouda, Performance analysis of proposed hybrid air conditioning and humidification–dehumidification systems for energy saving and water production in hot and dry climatic regions, Energy Convers. Manag. 96 (2015) 208–227, https://doi.org/10.1016/j.enconman.2015.02.082.
[36] R. Tariq, N.A. Sheikh, J. Xamán, A. Bassam, An innovative air saturator for humidification-dehumidification desalination application, Appl. Energy 228 (2018) 789–807, https://doi.org/10.1016/j.apenergy.2018.06.135.
[37] H.F. Elattar, A. Fouda, S.A. Nada, Performance investigation of a novel solar hybrid air conditioning and humidification–dehumidification water desalination system, Desalination 382 (2016) 28–42, https://doi.org/10.1016/j.desal.2015.12.023.
[38] G. Xiao, X. Wang, M. Ni, F. Wang, W. Zhu, Z. Luo, K. Cen, A review on solar stills for brine desalination, Appl. Energy 103 (2013) 642–652, https://doi.org/10.1016/j.apenergy.2012.10.029.
[39] J. Lindblom, B. Nordell, Underground condensation of humid air for drinking water production and subsurface irrigation, Desalination 203 (2007) 417–434, https://doi.org/10.1016/j.desal.2006.02.025.
[40] F. Incropera, D. DeWitt, Fundamentals of Heat and Mass Transfer, 4th ed., John Wiley & Sons, New York City, New York, 1996.
[41] R.E. Bolz, CRC Handbook of Tables for Applied Engineering Science, CRC Press, 1973.
[42] S.A. Kalogirou, Solar thermal collectors and applications, Prog. Energy Combust. Sci. 30 (2004) 231–295, https://doi.org/10.1016/j.pecs.2004.02.001.
[43] H.C. Hottel, A. Whillier, Evaluation of Flat-Plate Solar Collector Performance, (1955).
[44] S.A. Klein, Calculation of flat-plate collector loss coefficients, Sol. Energy 17 (1975) 79, 80, https://doi.org/10.1016/0038-092X(75)90020-1.
[45] H. Tabor, Radiation, Convection and Conduction Coefficients in Solar Collectors, (1958).
[46] A. Whillier, Solar Energy Collection and its Utilization for House Heating, Massachusetts Institute of Technology, 1953.
[47] A. Al-damook, W.H. Khalil, Experimental evaluation of an unglazed solar air collector for building space heating in Iraq, Renew. Energy 112 (2017) 498–509, https://doi.org/10.1016/j.renene.2017.05.051.
[48] J.A. Duffie, W.A. Beckman, Solar Engineering of Thermal Processes, 4th ed., John Wiley & Sons, 2013, https://doi.org/10.1002/9781118671603.
[49] W.C. Swinbank, Long-wave radiation from clear skies, Q. J. R. Meteorol. Soc. 89 (1963) 339–348, https://doi.org/10.1002/qj.49708938105.
[50] M.J. Moran, H.N. Shapiro, D.D. Boettner, M.B. Bailey, Fundamentals of Engineering Thermodynamics, 8th ed., wiley, 2014.
[51] Y.A. Çenge, M.A. Boles, Thermodynamics: An Engineering Approach, 8th ed., Mcgraw-Hill College, New York, 2015.
[52] B. Molineaux, B. Lachal, O. Guisan, Thermal analysis of five outdoor swimming pools heated by unglazed solar collectors, Sol. Energy 53 (1994) 21–26, https://doi.org/10.1016/S0038-092X(94)90599-1.

[53] M.K. Yau, R.R. Rogers, A Short Course in Cloud Physics, 3rd ed., © Butterworth-Heinemann, 1996.
[54] V.B. Sharma, S.C. Mullick, Estimation of heat-transfer coefficients, the upward heat flow, and evaporation in a solar still, J. Sol. Energy Eng. 113 (1991) 36–41.
[55] S. V B., M.S. C., Analysis of heat transfer coefficients and evaporation in a solar still, Int. J. Energy Res. 16 (2018) 517–531, https://doi.org/10.1002/er.4440160609.
[56] E. Sartori, Solar still versus solar evaporator: a comparative study between their thermal behaviors, Sol. Energy 56 (1996) 199–206, https://doi.org/10.1016/0038-092X(95)00094-8.
[57] A.E. Kabeel, Z.M. Omara, F.A. Essa, Improving the performance of solar still by using nanofluids and providing vacuum, Energy Convers. Manag. 86 (2014) 268–274, https://doi.org/10.1016/j.enconman.2014.05.050.
[58] H. Al-Hinai, M.S. Al-Nassri, B.A. Jubran, Effect of climatic, design and operational parameters on the yield of a simple solar still, Energy Convers. Manag. 43 (2002) 1639–1650, https://doi.org/10.1016/S0196-8904(01)00120-0.
[59] C. M, A. Yadav, Water desalination system using solar heat: a review, Renew. Sust. Energ. Rev. 67 (2017) 1308–1330, https://doi.org/10.1016/j.rser.2016.08.058.

Nomenclature

$A(m^2)$: Cross-section of solar humidifier, area of the collector plate surface
$A_r(m^2/m^2)$: The ratio of humidifier's coverage area to the area of solar still's bottom
$A_{sec}(m^2)$: Cross-section of inlet air of humidifier
$A_b(m^2)$: backside surface area of air collector
$A_c(m^2)$: frontal surface area of the air collector
$A_s(m^2)$: wall sides surface area of air collector
A_p: Perimeter area of the collector
C: Empirical factor defined in Eq. (5)
$C_{p,\ air} = 1005(J/kg.\ K)$: Specific heat of air
$C_w(J/K)$: Heat capacity of water
$D(m)$: Condenser tube diameter
$D_{AB}(m^2/s)$: Binary diffusion coefficient
$D_h(m)$: hydraulic diameter
f: Empirical factor defined in Eq. (6)
F_t: climate losses factor
F_{sh}: shadow factor
F_d: dust factor
$G(W/m^2)$: Solar heat gain
$G_t(W/m^2)$: Total (direct plus diffuse) solar energy incident on the collector aperture
$g_s(kg/s)$: Rate of the evaporated water
$h(kJ/kg)$: Enthalpy
$h_g(kJ/kg)$: Saturation vapor enthalpy
$h_c(W/m^2.\ K)$: Displacement heat transfer coefficient
$h_w(W/m^2.\ K)$: Surroundings displacement heat transfer coefficient, convection coefficient between the top glass and the environment Eq. (8)
$h_{water}(m)$: Height of water in solar still/humidifier
$h_m(m/s)$: Convection heat transfer
$h_{the}(W/m^2.\ K)$: theoretical forced convection heat transfer coefficient from the perforated absorber plate into airflow
$I_b(W)$: direct incident solar radiation
$k_{ins}(W/m.\ K)$: the thermal conductivity of insulation
$k_{air}(W/m.\ K)$: the thermal conductivity of airflow
$L(m)$: Condenser tube length, thickness of insulation (m^2)
$L_w(J/kg)$: Latent heat of water evaporation
$K_{bs} = 1.11(W/m^2.\ K)$: Coefficient for solar humidifier's total heat transfer to the surroundings
$M_a(kg/kmol)$: Molar mass of air
$M_d(kg/hr)$: Rate of distilled water
$M_w(kg/kmol)$: Molar mass of water
$\dot{m}(kg/s)$: Flow rate
N,M: Number of glass cover
Nu_{the}: theoretical Nusselt number
$P_{tot}(Pa)$: Total pressure
$P_{ws}(Pa)$: Minor air pressure in water-evaporating temperature
$q_{cond}(W/m^2)$: Condensation heat transfer
$q_{cw}(W)$: Convection heat transfer
$q_{ew}(W)$: Vaporization heat transfer
$q_{kw}(W/m^2)$: Conduction heat transfer
$q_{rw}(W/m^2)$: Radiation heat transfer
$q_u(W)$: Rate of useful energy delivered by the collector
$Q_B(W)$: Rate of energy conducted through the bottom insulation
$Q_E(W)$: Rate of energy loss due to edge effects
$Q_T(W)$: Rate of energy lost by radiation and convection to the glass covers above
$Q_{losses}(W/m^2)$: thermal losses
$Q_{abs}(W/m^2)$: thermal energy absorbed
s: Tilt of collector as measured from horizontal
Sh: Sherwood number
$T(°C)$: Heat temperature
$T_a(°C)$: Ambient temperature
$T_{air}(°C)$: Temperature of cycle's inflowing air
$T_p(°C, K)$: Temperature of condenser tube's walls, average temperature of the absorbing surface, perforated absorber plate temperature
$T_i(°C)$: Temperatures of the fluid entering the collector
$T_o(°C)$: Temperature of the fluid leaving the collector
$T_{out}(K)$: outlet air temperature from UTC
$T_{i,\ h}(°C)$: Temperature of water inlet the humidifier from flat plat solar collector
$T_{o,\ h}(°C)$: Temperature of water out let of the humidifier
$T_{water}(°C)$: Temperature of water at the bottom of solar humidifier
$T_w^{k+1}(°C)$: Temperature of water in the humidifier in the new time
$T_w^k(°C)$: Initial temperature of water in humidifier
$V,\ u_{air}(m/s)$: Airflow velocity
$X(m)$: Solar humidifier's length
$X_n(kg/kg)$: Specific humidity of saturation air in the temperature of humidifier's water
$X_s(kg/kg)$: Specific humidity of air in room temperature
$W(m/s)$: Wind speed
$U_L(W/m^2.\ K)$: Collector overall energy loss coefficient
$U_b(W/m^2.\ K)$: thermal losses from the backside of the system
$U_f(W/m^2.\ K)$: thermal losses of the frontal side of the system
$U_s(W/m^2.\ K)$: thermal losses of the edges of the system
$U_T(W/m^2.\ K)$: total thermal losses of the system
ϵ_p: Absorber plate emittance
ϵ_g: Emissivity of glass covers
$\alpha_w = 0.9$: Water absorption coefficient
$\alpha_p = 0.96$: perforated plate absorptivity(0.96)
$\rho_{v,\ s}(kg/m^3)$: Saturation vapor density
$\sigma = 5.67 * 10^{-8}(W/m^2K^4)$: Stefan–Boltzmann constant
$\tau\alpha$: Transmittance–absorptance product
η_h: hourly efficiency
$\tau_g = 0.9$: Glass transition coefficient
$\varphi(\%)$: Relative humidity
ω: Absolute humidity
$\Delta z(m)$: Spacing between tubes buried beneath the soil

Subscripts

a: Dry air
g: Glass coverage
i: Inlet
o: Outlet
S: Sky
v: Water vapor